Semi-Batch Homogeneous Catalytic In-Situ Spectroscopic Data. FTIR Spectral Reconstructions Using Band-Target Entropy Minimization (BTEM) without Spectral Preconditioning

Effendi Widjaja, Chuanzhao Li, and Marc Garland*

Department of Chemical and Environmental Engineering, 4 Engineering Drive 4, National University of Singapore, Singapore 119260

Received October 29, 2001

In the preceding paper in this issue, the concept of band-target entropy minimization (BTEM) was introduced, and it was successfully applied to spectral reconstruction from a stoichiometric organometallic reaction system after spectral preconditioning. In this contribution, the BTEM algorithm is reapplied to semi-batch homogeneous catalytic reactions without spectral preconditioning. The homogeneous catalytic hydroformylation of 3,3-dimethylbut-1-ene, starting with $Rh_4(\sigma\text{-}CO)_9(\mu\text{-}CO)_3$ as catalyst precursor in *n*-hexane as solvent, was studied at 298 K and variable total pressure, using high pressure in situ infrared spectroscopy as the analytical tool. The *non-preconditioned* data were then subjected to BTEM in order to recover the pure component spectra of the species present. The pure component spectra of background moisture and carbon dioxide, hexane, dissolved CO in hexane, and the dissolved species present, namely the organic reactant 3,3-dimethylbut-1-ene, the organic product 4,4-dimethylpentanal, the catalyst precursor $Rh_4(\sigma\text{-}CO)_9(\mu\text{-}CO)_3$, the observable organometallic intermediate $RCORh(CO)_4$, and $Rh_6(CO)_{16}$, were all readily recovered. An unexpected finding was a very well resolved spectrum with two terminal CO vibrations centered at 2068 and 2076 cm^{-1} (almost exactly overlapping with $Rh_4(\sigma\text{-}CO)_9(\mu\text{-}CO)_3$, but without bridging carbonyls). With reasonable certainty we are assigning this new spectrum to the previously unknown complex $Rh_4(\sigma\text{-}CO)_{12}$. The results indicate that spectral reconstruction, *using no libraries and no a priori information*, is indeed possible from semi-batch runs. This finding holds promise for rapid and cost-effective spectroscopic system identification of reactive organometallic and homogeneous catalytic systems.

Introduction

Recently, a new spectral reconstruction algorithm called band-target entropy minimization (BTEM) was applied to multiple-experiment spectroscopic data obtained from the well-known stoichiometric decomposition of $Rh_4(CO)_{12}$ to $Rh_6(CO)_{16}$.[1] The algorithm was able to readily recover the pure component solution spectra of the polynuclear organometallic species present, as well as the pure component spectrum of suspended and undissolved $Rh_6(CO)_{16}$ *without using any libraries or a priori information*. The sequence of matrices used and generated during the BTEM algorithm for multiple-experiment data is shown in eq 1. The matrix $\mathbf{A}^{exp}$ is

$$\mathbf{A}^{exp} \rightarrow \mathbf{A}^{pre} \rightarrow \mathbf{V}^{T} \rightarrow \mathbf{a}_{s\times\nu} \qquad (1)$$

the experimental absorbance, $\mathbf{A}^{pre}$ is the matrix of preconditioned data after spectral subtraction of background, solvent, etc., $\mathbf{V}^{T}$ is the matrix of right singular vectors, and $\mathbf{a}_{s\times\nu}$ is the matrix of reconstructed pure component spectra.[2]

Multiple experimental runs in organometallic chemistry, but particularly in homogeneous catalysis, are usually very time-consuming from a logistical viewpoint and expensive from a resources viewpoint (spectrometer time, complexes, ligands, reagents, etc.). Furthermore, a single experimental run is entirely insufficient for the BTEM algorithm (or for any other signal processing algorithm), since a single run cannot possibly span the vector space of observables. However, a single semi-batch experimental run would appear to satisfy both needs. Indeed, a single semi-batch experiment is considerably more frugal with resources, but at the same time, the data obtained at multiple reaction conditions will span the vector space of observables.

In the present contribution, we now reapply the BTEM algorithm to a homogeneous catalytic reaction: namely, the well-studied unmodified rhodium-catalyzed hydroformylation of alkenes—specifically using 3,3-dimethylbut-1-ene as substrate. A few different semi-batch experiments were performed (see Experimental Section). In each semi-batch experiment, the hydroformylation reaction is started, and then sequential additions of more reagents are made during the experiment. Since reference spectra of the solvent hexane and the dissolved carbon monoxide are not available at each

(1) Chew, W.; Widjaja, E.; Garland, M. *Organometallics* **2002**, *21*, 1982.

(2) Where s is the number of species present and ν is the number of spectroscopic channels.

10.1021/om010933j CCC: $22.00
Publication on Web 04/22/2002

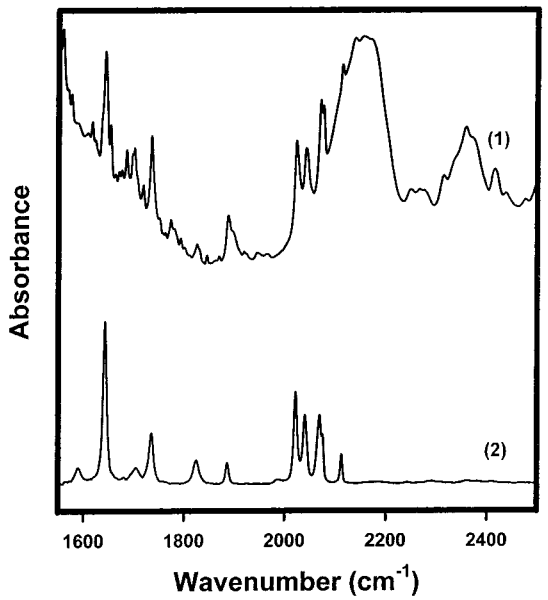

Figure 1. Comparison between a raw experimental spectrum and a numerically preconditioned spectrum: (1) raw experimental spectrum of the semi-batch experiment; (2) preconditioned spectrum of a previous study after subtracting solvent hexane, water, CO_2, and dissolved CO.

step of the semi-batch run, adequate spectral preconditioning cannot be performed. Therefore, in the present contribution the experimental absorbance matrix is used directly without spectral preprocessing of any sort (see Computational Aspects). The sequence of matrices used and generated in a semi-batch BTEM analysis can be written as

$$\mathbf{A}^{\exp} \rightarrow \mathbf{V}^{\mathrm{T}} \rightarrow \mathbf{a}_{s\times\nu} \qquad (2)$$

We have undertaken the present experimental and computational study using FTIR data, since it compliments our previous work on the rhodium-catalyzed hydroformylation reaction[3] and further illustrates the potential of spectroscopic system identification. Previously, the application of preconditioned BTEM to a multiple-experiment stoichiometric organometallic system was shown, and now the application of nonpreconditioned BTEM to a semi-batch homogeneous catalytic system is demonstrated. The present efforts using infrared spectroscopy are aimed at resolving many of the remaining issues and thereby open the opportunities for future semi-batch NMR studies as a relatively straightforward extension.

Results

Experimental Absorbance Data. An experimental absorbance spectrum from the third step of one *semi-batch* experiment, under the conditions of 2.0 MPa of CO and 2.0 MPa of H_2, is shown in curve 1 of Figure 1. This spectrum clearly shows the presence of water (high-frequency pattern at low wavenumbers) and a broad CO absorbance at ca. 2100 cm^{-1}. The complexity of these raw experimental data, compared to numerically preconditioned data, is seen by comparison to curve 2. The preconditioned spectrum was obtained by numerical subtraction of solvent hexane, background water, background CO_2, and dissolved CO. Preconditioning is difficult or impossible with *semi-batch* data, since appropriate reference spectra at each step are not available.

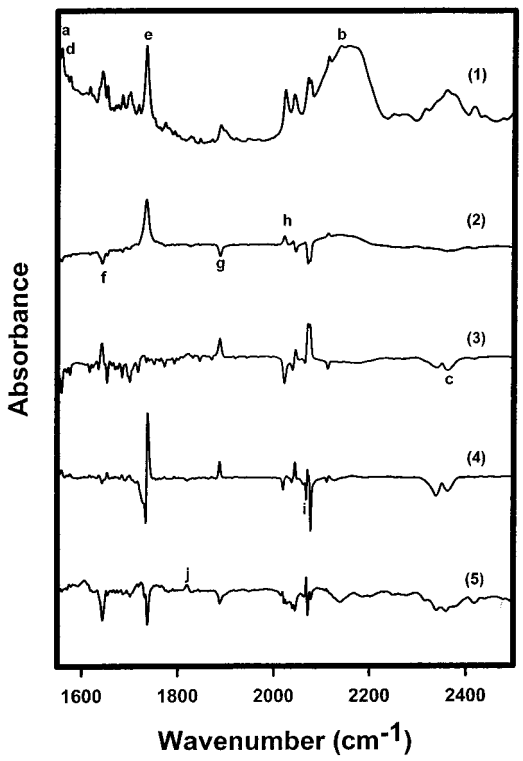

Figure 2. First few right singular vectors of the $\mathbf{V}^{\mathrm{T}}$ matrix: (1) first vector; (2) second vector; (3) fifth vector; (4) ninth vector; (5) tenth vector.

The BTEM algorithm was first applied to the semi-batch experiment involving seven steps. The quality of the reconstructed spectra was poor. Therefore, the raw spectroscopic data from the other two additional semi-batch experiments were included. This data set consisted of 250 spectra.

Singular Value Decomposition. Singular value decomposition was used to decompose the raw experimental *semi-batch* absorbance data matrix $\mathbf{A}_{250\times4751}$, yielding the orthonormal matrices $\mathbf{U}_{250\times250}$ and $\mathbf{V}^{\mathrm{T}}_{4751\times4751}$ and the diagonal singular value matrix $\Sigma_{250\times4751}$. The row vectors in the $\mathbf{V}^{\mathrm{T}}$ matrix are orthogonal basis vectors that contain the abstract information on the pure component spectra. Although a total of 4751 right singular vectors of $\mathbf{V}^{\mathrm{T}}$ were obtained after decomposition, only the first 250 $\mathbf{V}^{\mathrm{T}}$ vectors are physically meaningful, since only 250 reaction spectra are in the original data array $\mathbf{A}_{250\times4751}$. Five of the first 10 $\mathbf{V}^{\mathrm{T}}$ vectors are presented in Figure 2, while Figure 3 presents the 20th, 50th and 250th $\mathbf{V}^{\mathrm{T}}$ vectors.

The right singular vectors in the $\mathbf{V}^{\mathrm{T}}$ matrix are ordered according to their contribution to the total variance in the observations. Therefore, the first vector in Figure 2 is just the average spectrum—which clearly shows all the components and therefore looks very similar to curve 1 in Figure 1. The contribution of each additional right singular vector to the total variance of the data set decreases monotonically. Accordingly, in Figure 3 the signal-to-noise level is low in the 20th and

(3) (a) Garland, M.; Bor, G. *Inorg. Chem*. **1989**, *28*, 410. (b) Garland, M.; Pino, P. *Organometallics* **1991**, *10*, 1693. (c) Liu, G.; Garland, M. *Organometallics* **1999**, *18*, 3457.

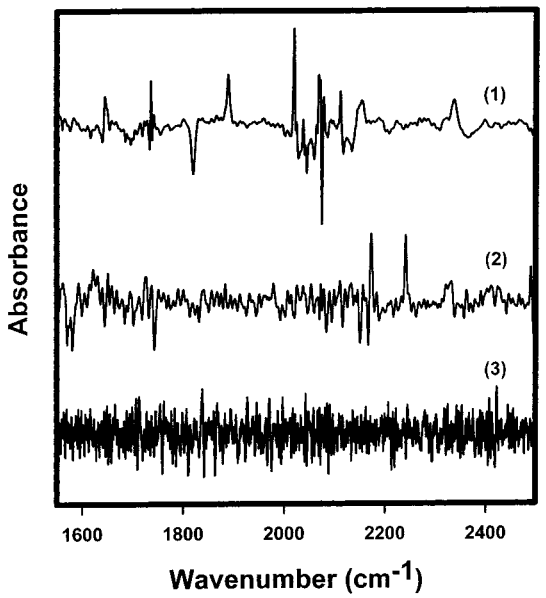

Figure 3. Another three right singular vectors of the $\mathbf{V}^T$ matrix: (1) 20th vector; (2) 50th vector; (3) 250th vector.

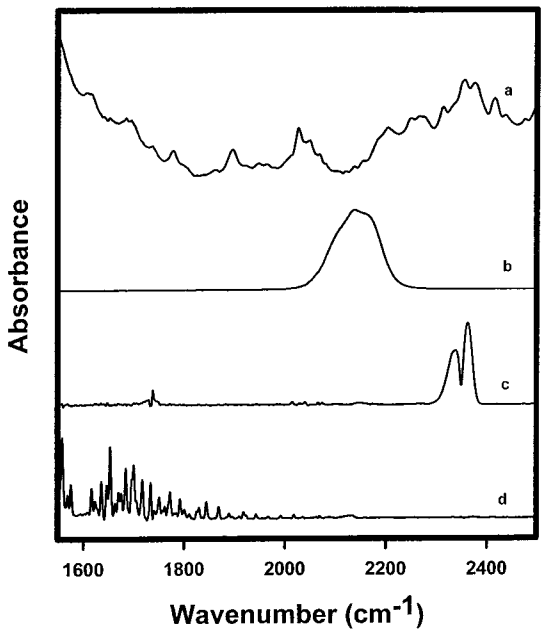

Figure 4. Reconstructed pure component spectra of major components: (a) *n*-C_6H_{14}; (b) CO; (c) CO_2; (d) H_2O.

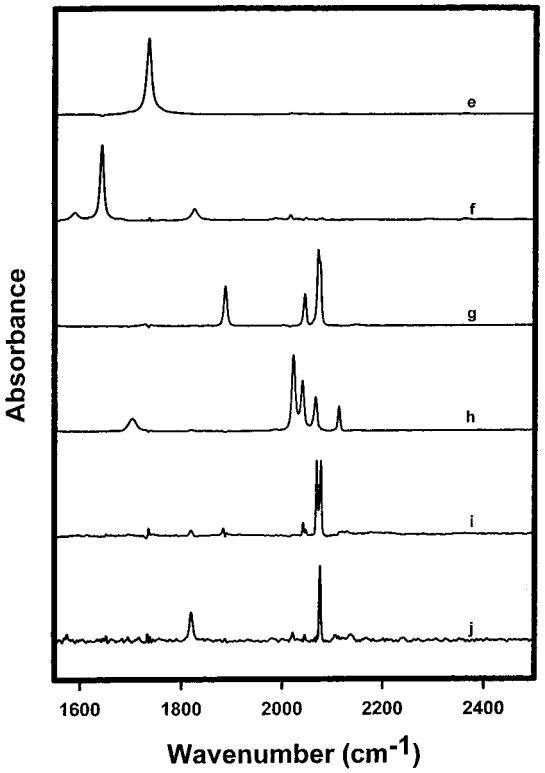

Figure 5. Reconstructed pure component spectra of minor components: (e) 44DMP; (f) 33DMB; (g) $Rh_4(\sigma\text{-}CO)_9(\mu\text{-}CO)_3$; (h) $RCORh(CO)_4$; (i) unknown species X; (j) $Rh_6(CO)_{16}$.

50th vectors, and essentially only randomly distributed white noise can be identified in the last right singular vector.

Pure Component Spectra Reconstruction Results via BTEM (Major Components). After decomposition, the right singular vectors of the $\mathbf{V}^T$ matrix were inspected for significant spectral features/extrema to be used as targets in the BTEM algorithm. From the first few $\mathbf{V}^T$ vectors shown, 10 extrema labeled a−j were chosen as indicated in Figure 2. Four major components, namely hexane, CO, CO_2, and water vapor were resolved by targeting the localized extrema a−d[4] and by using entropy minimization with ca. $z = 25$ vectors.[5] These components are shown in Figure 4. These components account for ca. 93% of the entire absorbance data. The spectral similarities of the estimates of hexane, CO, and CO_2 with real experimental references from this laboratory are in excess of 0.98 in all cases.[6] In addition, the pure spectra are very smooth. The values of the first-derivative entropies were 8.12, 6.98, 7.15, and 7.09.

Pure Component Spectra Reconstruction Results via BTEM (Minor Components). Besides resolving the major components with significant signals in the reaction spectra, the BTEM algorithm was also used to reconstruct the minor components. These minor components are identifiable by local spectral intensity in some of the right singular vectors, as seen in Figure 2. The extrema e−j are located at ca. 1734, 1642, 1886, 2021, 2068, and 1819 cm^{-1}.[7] Six minor components were resolved, using entropy minimization with usually ca. $z = 50$ vectors, as shown in Figure 5.[8] These pure component spectra clearly represent 4,4-dimethylpentanal, 3,3-dimethylbut-1-ene, $Rh_4(\sigma\text{-}CO)_9(\mu\text{-}CO)_3$, $RCORh(CO)_4$, a new and previously unknown species X, and $Rh_6(CO)_{16}$. The pure spectra are very smooth (with the exception of $Rh_6(CO)_{16}$). The values of the first-derivative entropies were 5.75, 6.49, 6.09, 6.30, 6.20, and 7.44, respectively.

A few pure component reconstructions, namely 3,3-dimethylbut-1-ene, the unknown species X, and Rh_6-

(4) $\alpha = 1.0$, $\alpha = 1.0$, $\alpha = 1.0$, and $\alpha = 1.0$ are used in eq 8 or eq 16 for the targeted regions 1550−1552, 2135−2140, 2360−2364, and 1558−1560 cm^{-1}, respectively.

(5) The average computational time for major component reconstruction, $z = 25$, is approximately 6 h.

(6) A well-established measure for similarity is defined by the inner product of the estimated spectrum and experimental spectrum in an L^2 norm. A value of identically 1 means that there is exact agreement.

(7) $\alpha = 1.0$, $\alpha = 1.0$, $\alpha = 3.0$, $\alpha = 1.0$, $\alpha = 1.0$, and $\alpha = 5.0$ are used in eq 8 or eq 16 for the targeted regions 1733−1735, 1640−1644, 1885−1887, 2020−2023, 2067.5−2068.5, and 1818−1820 cm^{-1}, respectively.

(8) The average computational time for minor component reconstruction, $z = 50$, is approximately 12 h.

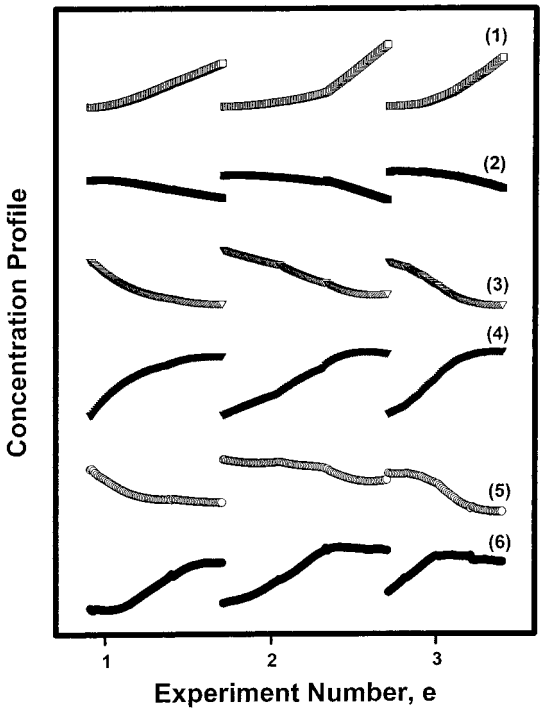

Figure 6. Relative concentration profile of reconstructed minor components for all three experiments: (1) 44DMP; (2) 33DMB; (3) $Rh_4(\sigma\text{-}CO)_9(\mu\text{-}CO)_3$; (4) $RCORh(CO)_4$; (5) unknown species X; (6) $Rh_6(CO)_{16}$.

$(CO)_{16}$, show some spectral artifacts. The estimate of 3,3-dimethylbut-1-ene shows some localized absorbance at ca. 2015 and 2300 cm^{-1}, which is associated with hexane (note the nonzero baseline). The estimate of the unknown species X shows some localized absorbance at ca. 1734, 1819, 1886, and 2042 cm^{-1}. The features at 1734 and 1886 cm^{-1} are clearly artifacts, as evidenced by the asymmetric sigmoid profiles of these bands. These features arise from the aldehyde and $Rh_4(\sigma\text{-}CO)_9(\mu\text{-}CO)_3$ present in solution. Such profiles are frequently obtained with many spectroscopic measurements when spectral subtractions are performed on nonstationary bands. The bands at 1819 and 2042 cm^{-1} are also artifacts.[9] The estimate of $Rh_6(CO)_{16}$ is not perfect because the true signal intensity is just above the noise level. In other words, considerable signal-to-noise enhancement was achieved during the BTEM reconstruction.

Relative Concentration Profiles of Minor Components. The normalized concentrations of all the components are automatically obtained from the BTEM algorithm (see Computational Aspects). Figure 6 shows the normalized concentrations of the minor components.

Discussion

Spectral Reconstructions, Concentration Profiles, and Integrated Intensity. In these semi-batch experiments, the pure component spectra of the major components such as hexane, CO, CO_2, and water vapor could be recovered directly by entropy minimization techniques. However, more importantly, the minor organic and organometallic species associated with the catalysis could be recovered using these three semi-batch experiments alone—without the use of any a priori information or spectral libraries. This was possible even though the concentrations involved are very low. For example, the estimated mean concentrations of $Rh_4(\sigma\text{-}CO)_9(\mu\text{-}CO)_3$ and $RCORh(CO)_4$ in this data set are only 39 and 80 ppm, respectively.

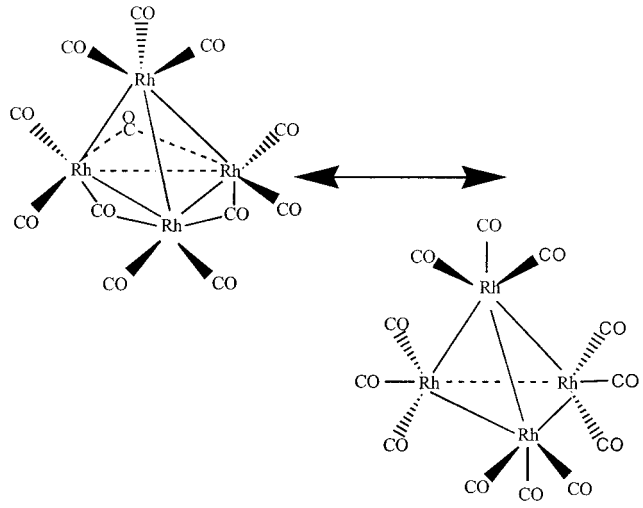

Figure 7. Structures of $Rh_4(\sigma\text{-}CO)_9(\mu\text{-}CO)_3$ and $Rh_4(\sigma\text{-}CO)_{12}$.

Inspection of the pure component spectrum for X indicates that it is a metal carbonyl. Indeed, the bands are very narrow (half-width of ca. 5 cm^{-1}). The spectrum is extremely similar to that of the precursor $Rh_4(\sigma\text{-}CO)_9(\mu\text{-}CO)_3$ in the terminal carbonyl region, and the residual signals in the bridging carbonyl regions appear to be artifacts.[9] Furthermore, the concentration profiles of the unknown species X in Figure 6 mirror the profiles of $Rh_4(\sigma\text{-}CO)_9(\mu\text{-}CO)_3$ in all experiments. This strongly suggests that the new species is in fact a tetranuclear rhodium carbonyl cluster with only terminal carbonyls—i.e., $Rh_4(\sigma\text{-}CO)_{12}$[10] (Figure 7).

The integrated intensities suggest the ratio of $Rh_4(\sigma\text{-}CO)_{12}$ to $Rh_4(\sigma\text{-}CO)_9(\mu\text{-}CO)_3$ is ca. 0.26 at 298 K. Thus, the free energy of $Rh_4(\sigma\text{-}CO)_{12}$ is ca. 3.3 kJ/mol higher than that of $Rh_4(\sigma\text{-}CO)_9(\mu\text{-}CO)_3$. This situation is remarkably similar to that for $Co_2(CO)_8$. The solid precursor has two bridging carbonyls, i.e. $Co_2(\sigma\text{-}CO)_6(\mu\text{-}CO)_2$, but the solution structure at room temperature consists of an equilibrium of both isomers $Co_2(\sigma\text{-}CO)_6(\mu\text{-}CO)_2$ and $Co_2(\sigma\text{-}CO)_8$, where the latter has a higher free energy.[11] It should be noted that the recovered spectra of $Rh_4(\sigma\text{-}CO)_{12}$ were generated from experiments where the estimated mean concentration is only 7 ppm.

(9) An additional set of multiple-experiment hydroformylation reactions were also carried out and preconditioned BTEM performed. Again, the unknown species X was recovered. However, in this case, the reconstructed pure component spectrum shows no residual absorbance at 1819 cm^{-1} and the sigmoid at 2042 cm^{-1} is even more pronounced.

(10) It was possible to resolve this new isomer of the catalyst precursor due to the pressure-induced variations present in the spectroscopic data set. The experimental design is important. The previous BTEM analysis of the stoichiometric reactions between rhodium carbonyl clusters[1] was unable to resolve this new isomer, since variations in temperature and/or pressure were not made, and hence, the spectrum of the new isomer remained imbedded in the "pure component" spectral reconstruction of $Rh_4(CO)_{12}$.

(11) (a) Bor, G. *Spectrochim. Acta* **1963**, *19*, 2065. (b) Noack, K. *Spectrochim. Acta* **1963**, *19*, 1925. (c) Noack, K. *Helv. Chim. Acta* **1964**, *47*, 1064.

Table 1. Percentage of Reconstructed Integrated Absorbance of Each Component Compared to the Total Original Experimental Data

component	reconstructed integrated abs compared to the total original exptl data, %
n-C_6H_{14}	61.392
CO	26.819
CO_2	0.837
H_2O	4.785
44DMP	3.100
33DMB	2.238
$Rh_4(\sigma\text{-}CO)_9(\mu\text{-}CO)_3$	1.255
$RCORh(CO)_4$	1.887
$Rh_4(\sigma\text{-}CO)_{12}$	0.324
$Rh_6(CO)_{16}$	0.237
total	102.88

The relative concentration profiles for the minor components (Figure 6) are exactly as expected. Indeed, the profiles of catalyst precursors $Rh_4(\sigma\text{-}CO)_9(\mu\text{-}CO)_3$ and $Rh_4(\sigma\text{-}CO)_{12}$ and the organic substrate 3,3-dimethylbut-1-ene decrease in time and the organometallic intermediate $RCORh(CO)_4$ and the organic product 4,4-dimethylpentanal increase. The concentration of $Rh_6(CO)_{16}$ is generally increasing (deactivation of unmodified rhodium hydroformylation reactions due to clusterification is well-known[12]). The two steps in the first semi-batch experiment, the three steps in the second semi-batch experiment, and the seven steps in the third semi-batch experiment can be clearly seen as discontinuities in the curves presented in Figure 6.

The total integrated intensities for the major and minor species for all the experiments are shown in Table 1. The data indicate that only ca. 9% of the data is due to the minor components. The total reconstructed absorbance is ca. 103% of the experimental intensity. This numerical result is primarily due to the fact that the reconstructed pure component spectra are mean representations over all observations. Thus, the pure spectra of $Rh_4(CO)_{12}$ in the first and last spectra of any semi-batch run are slightly different due to shifting band centers and changing band shape and the reconstruction is a convolution of these observations. Therefore, the pure component estimates of all species have slightly larger integrated intensity than any particular true component spectrum.

Maximizing Signal Recovery: Spectral Nonlinearities. Ten pure component spectra were recovered (4 major and 6 minor). Therefore, if the signals were stationary, only 10 vectors in $\mathbf{V}^T$ should have localized signals. This is clearly not the case. Localized features were found in the first 50 or more vectors. Therefore, serious spectral nonlinearities, such as changing band positions and band shapes, exist. The use of $z > s$ right singular vectors in the BTEM algorithm provided a means of maximizing signal recovery. In particular, it provided the means of recovering the major pure component spectra (with just $z = 25$) and the minor spectra (with $z = 50$). The use of more vectors allowed smoother and simpler pure component estimates for low concentration species. The integrated intensity of the lowest concentration species $Rh_6(CO)_{16}$ was only 0.24% of the original experimental semi-batch data.

Multiple Semi-Batch Runs versus a Single Semi-Batch Run. The present study was undertaken for two reasons. First, we wanted to avoid the computationally intensive preconditioning of data. More importantly, we wanted to reduce the number of experiments and therefore the cost of spectral identification in homogeneous catalytic studies. The preliminary analysis of the seven-step semi-batch experimental data indicated that only very rough spectral estimates were possible. The addition of two further sets of semi-batch data resulted in the excellent reconstructions presented in Figures 4 and 5.

The reason is now clear. One semi-batch experiment is sufficient for spectral reconstruction *if* it is properly designed. In the seven-step experiment, only two directions in the composition space were varied significantly—namely hydrogen and carbon monoxide. Sufficient variation was not achieved in other directions. A large perturbation induced by the addition of more solvent and/or more solvent and complex and/or more solvent and alkene would have ensured that the vector spaces of observations are properly spanned by the orthonormal right singular vectors. Therefore, proper experimental design should ensure the success of a single semi-batch analysis.

Conclusions

Full spectral recovery from a very dilute homogeneous catalyzed reaction, run in semi-batch mode, was achieved, given no libraries of other a priori information. All anticipated major and minor component spectra were reconstructed. BTEM spectral recovery of the rhodium-catalyzed hydroformylation of alkenes was successful, in the presence of significant solvent and background signals. In addition, the previously unknown and unstable polynuclear rhodium carbonyl species $Rh_4(\sigma\text{-}CO)_{12}$ was identified. Spectral preconditioning proved unnecessary. The present contribution shows that semi-batch data can be used for system identification. However, without proper experimental design, multiple semi-batch data sets are still needed instead of just one semi-batch experiment. This study clarifies the limitation but also the potential of semi-batch data for system identification and justifies future attempts to achieve spectroscopic system identification using extraordinarily useful single semi-batch NMR studies.

Experimental Section

General Information. All solution preparations were carried out under argon (99.9995%, Soxal, Singapore) using standard Schlenk techniques.[13] The argon was further purified prior to use by passage through de-oxy and zeolite columns. All reactions were carried out under carbon monoxide (99.97%, Soxal, Singapore) and hydrogen (99.999%, Soxal, Singapore) after further purification through de-oxy and zeolite columns.

The precious-metal complex $Rh_4(CO)_{12}$, with a stated purity of 98% minimum, was obtained from Strem Chemicals (Newport, MA) and was used without further purification, although trace quantities of the high-nuclearity cluster $Rh_6(CO)_{16}$ are virtually always present. The n-hexane solvent (stated purity >99.6%, Fluka AG) was refluxed over sodium potassium alloy

(12) Kagan, Y. B.; Slivinskii, E.; Kurkin, V. L.; Korneeva, G. A.; Aranovich, R. A.; Fal'kov, I. G.; Rzhevskaya, N. N.; Loktev, S. M.; *Neftekhimiya* **1985**, *25*, 791; *Chem. Abstr.* **1986**, *104*, 56974d.

(13) Shriver, D. F.; Drezdzon, M. A. *The Manipulation of Air-Sensitive Compounds*; Wiley: New York, 1986.

under argon. 3,3-Dimethylbut-1-ene (99%,Fluka AG, Switzerland) was used as obtained.

Equipment. In-situ spectroscopic studies were performed in a 1.5 L stainless steel (SS316) autoclave (Büchi-Uster, Switzerland) which was connected to a high-pressure infrared cell. The autoclave (P_{max} = 22.5 MPa) was equipped with a packed magnetic stirrer with six-bladed turbines in both the gas and liquid phases (Autoclave Engineers, Erie, PA) and was constructed with a heating/cooling mantle. A high-pressure membrane pump (Model DMK 30, Orlita AG, Geissen, Germany) with a maximum rating of 32.5 MPa and a 3 L/h flow rate was used to circulate the *n*-hexane solutions from the autoclave to the high-pressure IR cell and back to the autoclave via jacketed $^1/_8$ in. (SS316) high-pressure tubing (Autoclave Engineers). The entire system, autoclave, transfer lines, and infrared cell, was cooled using a Polyscience Model 9505 cryostat and could be maintained isothermal ($\Delta T \leq 0.5$ °C) at 298−313 °C. Temperature measurements were made at the cryostat, autoclave, and IR cell with PT-100 thermoresistors. The necessary connections to vacuum and gases were made with $^1/_4$ in. (SS316) high-pressure tubing (Autoclave Engineers), and 1.0, 5.0, and 10.0 piezocrystals were used for pressure measurements (Keller AG, Winterthur, Switzerland). The entire system was gastight under vacuum as well as at 20.0 MPa, the maximum operating pressure.

The high-pressure infrared cell was constructed at the ETH-Zürich of SS316 steel and could be heated and cooled. The CaF_2 single-crystal windows (Korth Monokristalle, Kiel, Germany) had dimensions of 40 mm diameter by 15 mm thickness. Two sets of Viton and silicone gaskets provided sealing, and Teflon spacers were used between the windows. The construction of the flow-through cell[14] is a variation on a design due to Noack[15] and differs in some respects from other high-pressure infrared cells described in the literature (for a review, see Whyman[16]). The high-pressure cell was situated in a Perkin-Elmer 2000 FTIR infrared spectrometer. The cell chamber was purged with purified nitrogen (99.999%, Soxal, Singapore). The resolution was set to 4 cm^{-1} for all spectroscopic measurements. A schematic diagram of the experimental setup can be found in ref 17.

In-Situ Spectroscopic and Kinetic Studies. All semi-batch experiments were initiated in the following manner. First 200 mL of *n*-hexane was transferred under argon to the autoclave. The total system pressure was raised to 1.0−2.0 MPa of CO, and the stirrer and high-pressure membrane pump were started. A solution of 5−8 mL of 3,3-dimethylbut-1-ene (33DMB) dissolved in 50 mL of *n*-hexane was prepared, transferred to the high-pressure reservoir under argon, pressured with CO, and then added to the autoclave. A solution of 78−103 mg of $Rh_4(CO)_{12}$ dissolved in 50 mL of *n*-hexane was prepared, transferred to the high-pressure reservoir under argon, pressured with CO, and then added to the autoclave. Hydrogen (1.0 MPa) was then added to initiate the synthesis. Spectra were recorded at regular intervals (a few minutes) in the range 1000−2500 cm^{-1}, for a total of ca. 70−100 spectra in each of the three experiments.

In these three semi-batch experiments, the partial pressures of carbon monoxide and hydrogen were repeatedly changed (ca. every 60−150 min). The step sizes were 1.0 or 2.0 MPa each time, starting with CO followed by hydrogen. In the first semi-batch experiment two steps were performed, in the second experiment three steps were performed, and in the third experiment seven steps were performed.

(14) Dietler, U. K. Dissertation 5428, ETH-Zurich, 1974.
(15) Noack, K. *Spectrochim. Acta* **1968**, *24A*, 1917.
(16) Whyman, R. In *Laboratory Methods in Vibrational Spectroscopy*, 3rd ed.; Willis, H. A., van der Maas, J. H., Miller, R. G. J., Eds., Wiley: New York, 1987; Chapter 12.
(17) Feng, J.; Garland, M. *Organometallics* **1999**, *18*, 417.

Computational Aspects

Computation. All algorithms were implemented in MATLAB. Calculations were performed on a WinNT Pentium III Xeon Work Station having two 450 MHz processors with 2 GB of RAM.

Spectral Analysis. The consolidated matrix of reaction absorbance data is denoted $\mathbf{A}_{ke\times\nu}$, where *k* denotes the number of spectra in one experiment, *e* denotes the number of experiments, and ν is the number of data channels associated with the experimental FTIR wavenumber range and interval taken.

According to the Lambert−Beer−Bouger law, the absorbance matrix is a linear product of the concentration matrix $\mathbf{C}_{ke\times s}$ (which incorporates the path length *l*) and absorptivity matrix $\mathbf{a}_{s\times\nu}$. This absorbance data matrix $\mathbf{A}_{ke\times\nu}$ can be subjected to singular value decomposition (SVD) (eq 3),[18] to obtain its

$$\mathbf{A}_{ke\times\nu} = \mathbf{C}_{ke\times s}\mathbf{a}_{s\times\nu} + \epsilon_{ke\times\nu} = \mathbf{U}_{ke\times ke}\Sigma_{ke\times\nu}\mathbf{V}^{\mathrm{T}}_{\nu\times\nu} \qquad (3)$$

$$\mathbf{A}_{ke\times\nu} \approx \hat{\mathbf{C}}_{ke\times s}\hat{\mathbf{a}}_{s\times\nu} = \mathbf{U}_{ke\times s}\Sigma_{s\times z}\mathbf{T}^{-1}_{s\times z}\mathbf{T}_{s\times z}\mathbf{V}^{\mathrm{T}}_{z\times\nu} \qquad ke \geq z \geq s \qquad (4)$$

$$\hat{\mathbf{C}}_{ke\times s} = \mathbf{U}_{ke\times s}\Sigma_{s\times z}\mathbf{T}^{-1}_{s\times z} = \mathbf{A}_{ke\times\nu}\hat{\mathbf{a}}^{\mathrm{T}}_{\nu\times s}(\hat{\mathbf{a}}_{s\times\nu}\hat{\mathbf{a}}^{\mathrm{T}}_{\nu\times s})^{-1} \qquad (5)$$

abstract orthonormal matrices $\mathbf{U}_{ke\times ke}$ and $\mathbf{V}^{\mathrm{T}}_{\nu\times\nu}$ with its singular matrix $\Sigma_{ke\times\nu}$. Furthermore, $\mathbf{A}_{ke\times\nu}$ can be approximated by eq 4, where *s* is the number of species recovered and *z* is the number of right singular vectors used for spectral reconstruction. Note that $\mathbf{T}^{-1}_{s\times z}$ is the generalized inverse for a rectangular matrix, $\hat{\mathbf{a}}_{s\times\nu}$ is the matrix of averaged pure component expectations for *s* species, $\hat{\mathbf{C}}_{ke\times s}$ is its corresponding expectation for concentration calculated from eq 5, and $\epsilon_{ke\times\nu}$ is a combination of experimental error and spectral nonlinearities.[19]

Instead of solving all rows of the transformation matrix $\mathbf{T}_{s\times z}$ at once, the BTEM algorithm solves the problem one transformation row at a time (see the following subsection for details), and hence, one spectrum at a time is resolved. The expectation for each spectrum $\hat{\mathbf{a}}_{1\times\nu}$ is then given by eq 6, with the corresponding expectation for the concentration $\hat{\mathbf{C}}_{ke\times 1}$ given by eq 7.

$$\hat{\mathbf{a}}_{1\times\nu} = \mathbf{T}_{1\times z}\mathbf{V}^{\mathrm{T}}_{z\times\nu} \qquad z \geq s \qquad (6)$$

$$\hat{\mathbf{C}}_{ke\times 1} = \mathbf{A}_{ke\times\nu}\hat{\mathbf{a}}^{\mathrm{T}}_{\nu\times 1}(\hat{\mathbf{a}}_{1\times\nu}\hat{\mathbf{a}}^{\mathrm{T}}_{\nu\times 1})^{-1} \qquad (7)$$

The objective function for optimizing the elements of $\mathbf{T}_{1\times z}$ in the BTEM algorithm is shown in eq 8.

$$\min G = -\sum_{\nu} h_\nu \ln h_\nu + P(\hat{\mathbf{a}}_{1\times\nu}, \hat{\mathbf{C}}_{ke\times 1}, \hat{\mathbf{a}}^{\max}_{1\times\nu}) \qquad (8)$$

where

$$h_\nu = \frac{\left|\frac{d\hat{a}_\nu}{d\nu}\right|}{\sum_{\nu}\left|\frac{d\hat{a}_\nu}{d\nu}\right|} \qquad (9)$$

$$P(\hat{\mathbf{a}}_{1\times\nu}, \hat{\mathbf{C}}_{ke\times 1}, \hat{\mathbf{a}}^{\max}_{1\times\nu}) = \gamma_a F_1(\hat{a}_\nu) + \gamma_c F_2(\hat{C}_{ke}) + \gamma_{\max} \qquad (10)$$

where

(18) Golub, G. H.; Van Loan, C. F. *Matrix Computations*; Johns Hopkins University Press: Baltimore, MD, 1996.
(19) Garland, M.; Visser, E.; Terwiesch, P.; Rippin, D. W. T. *Anal. Chim. Acta* **1997**, *351*, 337.

$$F_1(\hat{a}_\nu) = \sum_\nu (\hat{a}_\nu)^2 \; \forall \; \hat{a}_\nu < 0 \tag{11}$$

$$F_2(\hat{C}_{ke}) = \sum_{ke} (\hat{C}_{ke})^2 \; \forall \; \hat{C}_{ke} < 0 \tag{12}$$

$$\gamma_a = \begin{cases} 0 & F_1(\hat{a}_\nu) < \lambda_1 \\ 10 & \lambda_1 \le F_1(\hat{a}_\nu) < \lambda_2 \\ 10^4 & F_1(\hat{a}_\nu) \ge \lambda_2 \end{cases} \tag{13}$$

$$\gamma_c = 10^3 \; \forall \; F_2(\hat{C}_{ke}) \tag{14}$$

$$\gamma_{\max} = \begin{cases} 10^4 & \hat{\mathbf{a}}_{1\times\nu}^{\max} > \alpha \\ 0 & \hat{\mathbf{a}}_{1\times\nu}^{\max} \le \alpha \end{cases} \tag{15}$$

The first term on the right-hand side is the Shannon entropy function based on a first derivative of the absorbance estimate $\hat{\mathbf{a}}_{1\times\nu}$ (eq 9). The second term is a penalty function (eq 10) for ensuring (i) that there are non-negativities in each pure component spectral estimate $\hat{\mathbf{a}}_{1\times\nu}$ and each component estimated concentration $\hat{\mathbf{C}}_{ke\times1}$ and (ii) that a reasonable maximum spectral absorbance $\hat{\mathbf{a}}_{1\times\nu}^{\max}$ is obtained. Together with the penalty function are three sets of associated scalar parameters: (i) γ_a, γ_c, and $\gamma_{\max}$ are penalty coefficients for constraints defined by eqs 13−15, (ii) $\lambda_1 = 10^{-3}$ and $\lambda_2 = 10^{-2}$ are bounds for the absorptivity constraint defined in eq 13, and (iii) α defined in eq 15 sets the maximum absorbance of the resolved pure spectrum, in relation to the target band peak absorbance $\hat{\mathbf{a}}_{1\times\nu}^{\text{target}}$, which is normalized to be identically 1.0 (see following subsection).

In addition to the objective function based on information entropy minimization, some new objective functions with the nature to simplify the resolved bands of pure component spectra could be utilized. These new objective functions include the minimization of the summation of the first-, second-, or fourth-order derivative of the absorbance estimate $\hat{\mathbf{a}}_{1\times\nu}$ and minimization of the integrated area of the absorbance estimate $\hat{\mathbf{a}}_{1\times\nu}$ in order to prevent the over-resolution of the pure component spectra:

$$\min F_{\text{obj}} = \sum_\nu |ds_\nu| + \sum_\nu |\hat{a}_\nu| + P(\hat{\mathbf{a}}_{1\times\nu}, \hat{C}_{ke\times1}, \hat{\mathbf{a}}_{1\times\nu}^{\max}) \tag{16}$$

$$ds_\nu = \frac{d^n \hat{a}_\nu}{d\nu^n} \qquad n = 1, 2, 4 \tag{17}$$

The integrated area of $\hat{\mathbf{a}}_{1\times\nu}$ estimate is evaluated using numerical approach, such as the trapezoidal rule or Simpson's rule.

Band-Target Entropy Minimization (BTEM) Algorithm. In this method, the vectors in the $\mathbf{V}^T$ matrix were first inspected for significant spectral features. Such features usually appear only in the first few vectors of $\mathbf{V}^T$, as they represent most of the variance in the data matrix $\mathbf{A}_{ke\times\nu}$. Since BTEM targets these features one at a time, narrow intervals corresponding to these local extrema are assigned.

For example, the characteristic bridging carbonyl band for $Rh_4(CO)_{12}$ occurs at ca. 1886 cm^{-1}. Therefore, upon visual inspection, clearly identifiable spectral features/extrema can be seen at ca. 1886 cm^{-1} in the initial five $\mathbf{V}^T$ vectors. Accordingly, one sets the BTEM algorithm to target the interval 1885−1887 cm^{-1}. The algorithm then reconstructs the simplest function associated with this spectral feature such that the constraints imposed by eqs 10−15 are met.

The reason for taking a region of wavenumber for the targeted band rather than an exact singular band peak wavenumber is that *nonlinearities* due to band shifting and shape changes exist in real spectra. In the process of transforming the right singular vectors, the targeted band peak absorbance $\hat{\mathbf{a}}_{1\times\nu}^{\text{target}}$ is normalized to 1.0, and the maximum of the estimated spectrum $\hat{\mathbf{a}}_{1\times\nu}^{\max}$ is constrained to be equal to or less than the preassigned scalar value $\alpha \ge 1.0$ (eq 15). It is worth reiterating that no a priori information as such is required by this BTEM approach: only visual inspection of the right singular vectors.

Corana's Simulated Annealing. Corana's simulated annealing algorithm was employed to perform the global optimizations of the highly nonlinear BTEM objective function. Corana's simulated annealing is a random optimization method, modified from the original simulated annealing algorithm,[20] with dynamic step size generation and strict convergence criterion enhancements.[21] This algorithm has been extensively used and has proven capable of obtaining global solutions for highly nonlinear optimization problems.[22] A key feature of Corana's algorithm is its ability to escape local minima. This feature is based on the Metropolis selection criteria.

OM010933J

(20) Kirkpatrick, S.; Gelatt, C., Jr.; Vecchi, M. *Science* **1983**, *220*, 671.

(21) Corana, A.; Marchesi, M.; Martini, C.; Ridella, S. *ACM Trans. Math. Software* **1987**, *13*, 263.

(22) (a) Goffe, W. L.; Ferrier, G. D.; Rogers, J. *J. Econometrics* **1994**, *60*, 65. (b) Asprey, S. P.; Batres, R.; Fuchino, T.; Naka, Y. *Ind. Eng. Chem. Res.* **1999**, *38*, 2364. (c) Asprey, S. P.; Naka, Y. *J. Chem. Eng. Jpn.* **1999**, *32*, 328.